Synthesis, Characterization and Application of Zero-Valent Silver nano Adsorbents

Siva Sundarajan[1], Sulaiman Muhammad Sameem [2], Sudharsan Sankaranarayanan[3], Sayeekannan Ramaraj[*1]

PG Research and Department of chemistry, Thiagarajar College, Madurai-625 009, India [1]

Block Research Teacher Educator, SSA, Madurai-625008, India [2]

Department of Chemistry, PSR Engg College, Sivakasi- 626 140, India [3]

Abstract: The main objective of this study is to synthesize silver nanoparticles *via* green approach (environmentally eco friendly method) without using hazardous compounds. Here we present the distinctive properties of the silver nanoparticles (AgNPs) synthesized using hot water Phyllanthus emblica leaf extract (PELE) a reducing and capping agent. The nature of AgNPs synthesized was analyzed by atomic force microscope (AFM), scanning electron microscope (SEM), energy-dispersive microanalysis (EDX), X-ray diffraction spectroscopy (XRD), flourier transform infra red (FTIR), thermo gravimetric analysis (TGA), differential thermal analysis (DTA) and UV–vis spectroscopy (UV). We explored the ability of the AgNPs for removing Hg^{2+} from aqueous solution. Moreover, adsorption isotherms, kinetics and thermodynamics were studied to understand the mechanism of the synthesized AgNPs adsorbing metal ions. The adsorption isotherms were well described by Langmuir isotherm model with correlating constant (R^2) higher than 0.9945. The maximum adsorption capacity was determined at 303 K and was found to be 312 mg/g for Hg (II) ion respectively. The adsorption kinetics data were well fitted by the pseudo-second-order rate model with high regression coefficient (0.998). The intra particle diffusion of Hg (II) on AgNPs represents the rate-limiting step. The adsorption capacity was decreased with the increase of temperature, and thermodynamic calculations suggested that the adsorption of Hg (II) ions onto AgNPs is an exothermic process. It has been found that AgNPs show high selectivity's and adsorption capacities to removal of Hg^{2+} from its aqueous solution.

Keywords: Adsorption isotherms, Kinetics, Mercury, Thermodynamics, Phyllanthus emblica, silver nanoparticles, biological reduction, green synthesis.

I. INTRODUCTION

Nanotechnology is a rapidly expanding and potentially beneficial field with tremendous implications for society, industry, and medicine. The uses for nano-sized particles are even more remarkable. Silver nanoparticles have been synthesized using various plant extracts such as Hibiscus rosa sinensis [1], Svensonia hyderabadensis [2], Trianthema decandra [3], Dioscorea batatas [4], Moringa oleifera [5], Bacopa monniera [6], Citrus limon [7], Arbutus unedo [8], Acalypha indica [9], Mentha piperita [10], Cassia auriculata [11] etc. so for the AgNPs (zero-valent metal) are not synthesized using PELE. Hence, we report an inexpensive, versatile, and very reproducible method for the large -scale synthesis of silver nanoparticles by reduction process using PELE. This is act both as reducing and stabilizing agent. Further, the contamination of water recourses by heavy metal is a serious worldwide environmental problem [12]. Numerous metals such as mercury, cadmium, chromium, lead, etc. are known to be significantly toxic. Mercury is well known for its extremely high toxicity. A very low concentration of mercury in water may cause health hazard. The World Health

Organization (WHO) has set the guideline value for inorganic mercury in drinking water at 1.0µgL−1 [13].These facts have motivated many physicochemical methods for heavy metal removal from aqueous solution, including chemical precipitation, membrane separation, electrochemical reduction, ion exchange, and adsorption [14−18]. Among these methods, adsorption is generally preferred for the removal of heavy metal ions due to its high efficiency, easy handling, availability of different adsorbents and cost effectiveness. Several types of materials, such as activated carbons [19], clay minerals [20], chelating materials [21], and chitosan/natural zeolites [22] have been researched to adsorb metal ions from aqueous solutions. Although traditional sorbents could remove heavy metal ions from wastewater, the low sorption capacities and efficiencies limit their application deeply. To solve these defects of traditional sorbents, nanomaterials are used as the novel ones to remove heavy metal ions in wastewater. Materials with the particle size between 1 nm to 100 nm are defined as nanomaterials. With novel size- and shape-dependent properties, nanomaterials have been extensively investigated over a decade [23]. In recent years, the development of nanoscience and nanotechnology has shown remarkable potential for the remediation of environmental problems [24]. Compared with traditional materials, nanostructure adsorbents have exhibited much higher efficiency and faster rates in water treatment. The generally used nanoparticles include zero-valent metals [25−32] to remove heavy metal ions from aqueous solution. From the literature survey, it is found that the application of PELE capped AgNPs (zero-valent metal) for adsorbing heavy metals has not been reported yet. Hence in the present study, we have synthesized these PELE capped AgNPs and applied these AgNPs for adsorbing heavy metals from aqueous solution. Meanwhile the influence of experimental parameters such as contact time, initial concentration and thermodynamics on adsorption will be revealed.

II. EXPERIMENTAL

A. Materials

The raw plant material used in the present study was Phyllanthus emblica (P.emblica).This is a plant material freely available in Tamil Nadu, India. AR grade SD fine silver nitrate ($AgNO_3$) was purchased and its 0.1 M solution was prepared in stock and diluted to 1 mM solution. The other chemicals and reagents were of chemically pure grade (AnalaR) procured from SD Fine Chemicals, India.

B. Methods

1) Preparation of PELE: Fresh P.emblica leaves were collected and washed with sterile distilled water and dried. After drying cut in to small pieces. The extract was prepared by taking 20 g of thoroughly washed finely cut P.emblica leaves in a 250-mL Erlenmeyer flask with 100 mL of deionized water, and then boiling the mixture at 60°C for 5 min. After boiling, the solution was decanted and filtered through nylon mesh (spectrum). The filtrate is used as reducing agent and stabilizer, stored at 4ºC for further nanoparticles synthesis process.
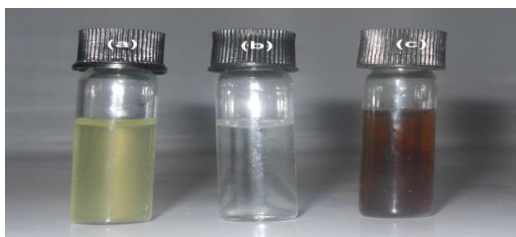

Fig. 1 (a) Leaf extracts (b) Silver nitrate mixture before and (c) After the synthesis of AgNPs

2) Green synthesis of AgNPs: For synthesis process, the PELE of 2 mL was added to 25 mL of 1 mM $AgNO_3$ aqueous solution and the resulting solution became brown in color. Then the mixture was stirred for 30 min to obtain the AgNPs.

Here the formation of AgNPs was identified by change in the color of the stock solution to brown within 20 min (Fig.1). Further the extract and aqueous solution ratio was varied. These biologically-reduced aqueous solutions of Ag nanoparticles were used for further characterizations. This process carried out at room temperature.

3) Spectral analysis: The synthesized AgNPs were confirmed by sampling the aqueous component of different time intervals and the absorption maxima was scanned by UV-Vis spectrophotometer at the wavelength of 300-800 nm on UV-1800 SHIMADZU spectrophotometer. The infrared spectra were achieved in a Shimadzu FT-IR spectrophotometer IR Affinity-1 by employing KBr pellets and registering amplitude waves ranging from 400 to 4000 cm^{-1}.

4) Morphological analysis: Morphological analysis was done using Philips model CM 200 SEM machine. Thin films of the sample were prepared on a carbon coated copper grid by just dropping a very small amount of the grid, extra solution was removed using a blotting paper and then the films on the SEM grid were allowed to dry by putting it under mercury lamp for 5 min.

5) Structural analysis: The formation and quality of compounds were checked using X'Pert Pro Materials Research diffractometer system. The X-ray diffraction (XRD) pattern was measured by drop coated films of AgNO$_3$ on glass plate and employed with characteristic radiation in the range of 20^0 to 90^0 at a scan rate of 0.05^0/min with the time constant of 2 s, CuK$_\alpha$ radiation and amplitude wave $\lambda = 1.5418$ Å working with a 40 kV voltage and 30 mA current. The full–width at half–maximum (FWHM) from three different peaks were used in Scherrer's equation to determine the average crystallite size of the nanoparticles.

6) AFM analysis: A small volume of sample was spread on a well cleaned glass cover slip surface mounted on the AFM stub, and dried with nitrogen flow at room temperature. Images were obtained in tapping mode using a silicon probe cantilever and resonance frequency 209-286 KHz, spring constant. The scan rate used was 1 HKz. A minimum of five images for each sample were obtained with AFM and analyzed to ensure reproducible results.

7) Batch adsorption studies: Adsorption studies were carried out in a batch mode by shaking 0.025 g AgNPs in 40 mL solution of Hg (II) with concentration range from 30 to 150 ppm onto the water bath shaker at 100 rpm stirring speed. Furthermore the adsorption studies were also carried out by varying time interval (10–50 min.) at 60 ppm concentration of Hg (II) to optimize the time required for the removal of Hg (II) from aqueous solution. The Hg (II) concentration in the supernatants after the adsorption onto the AgNPs was determined by using standard titration techniques as per the literature [33]. The equilibrium adsorption capacity of AgNPs was estimated with the help of following equation:

$$q_e \quad = \quad (C_o - C_e) \times V / M \qquad \text{-------------- (1)}$$

Where q_e is the equilibrium adsorption capacity (mg g^{-1}), C_e is the metal ion concentration (mg L^{-1}) at equilibrium, V is the volume of solution (L) and M is the weight (g) of adsorbent.

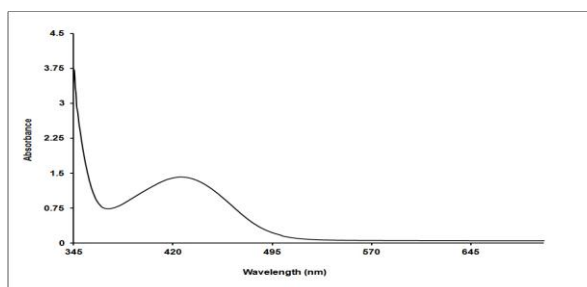## III. RESULTS AND DISCUSSION

A. *Spectral characterization*

Fig.2. UV-Visible Spectra of the synthesized AgNPs

1) UV–Vis spectra: The colour change in reaction mixture (metal ion solution + PELE) was recorded through visual observation. The color change showed the presence of silver nanoparticles in the leaf extract and it was characterized by UV-Visible spectrophotometer. The strong surface plasmon resonance band positioned at 420 nm was observed for AgNPs (Fig.2). The position of SPR band in UV–Vis spectra is sensitive to particle shape, size, its interaction with the medium, local refractive index and the extent of charge transfer between medium and the particles. The broad spectra indicate the presence of particles with a broad size distribution [34].
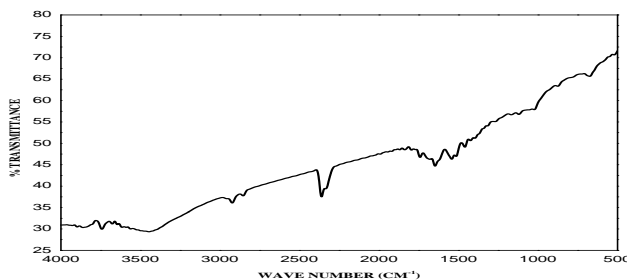

Fig.3. IR Spectra of the synthesized AgNPs

2) FT-IR spectra: FT-IR spectroscopy is used to probe the chemical composition of the surface of the AgNPs and the local molecular environment of the capping agents on the nanoparticles. The FT-IR spectrum of PELE mediated AgNPs is shown in Fig. 3. The band at 3446 cm^{-1} corresponds to intermolecular O-H stretching vibrations. The peaks at 2956 and 2922 cm^{-1} are belonging to C-H aromatic stretching frequencies. The medium absorption peak located at 1647 & 1680 cm^{-1} is identified as the amide group. This amide band occurs due to carbonyl stretch and N–H deformation vibrations in the amide linkage of proteins present in it. The band observed at 1460 & 1425 cm^{-1} may be due to the C–O–H vibrations. The band at 1269 cm^{-1} is assigned to polyphenols. The band at 2360 cm^{-1} corresponds to C–N stretching vibrations of aliphatic amines [35]. All these bands clearly confine the presence of polyphenols, proteins, tannins and flavonoids in PELE which act as reducing agents for the synthesis of silver nanoparticles. Thus, the IR spectroscopic study confirmed that the PELE has the ability to perform dual functions of reduction and stabilization of AgNPs.
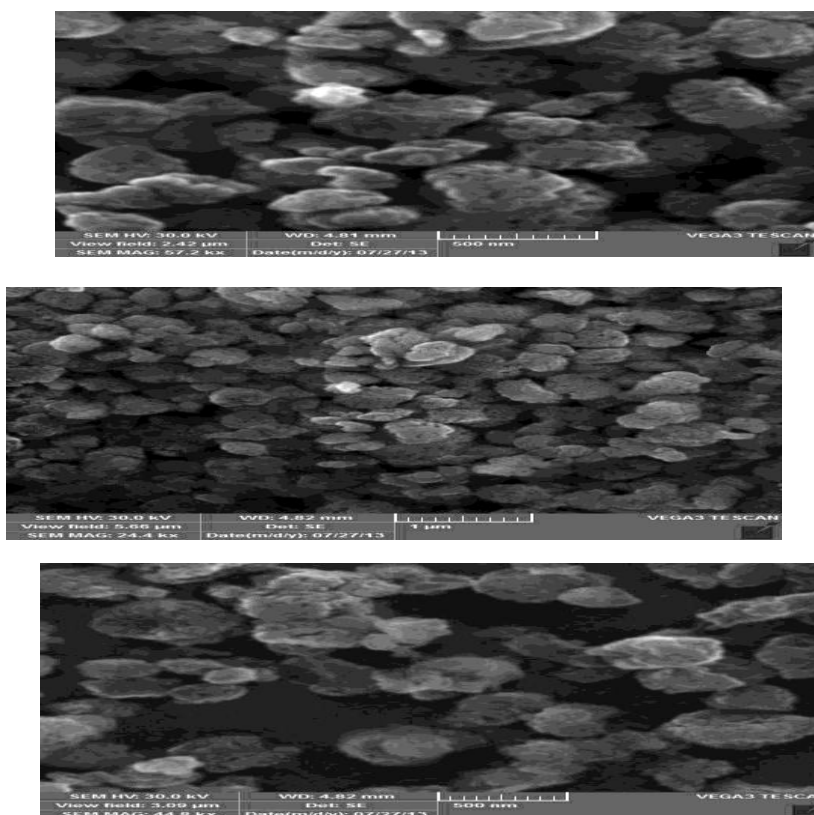
Fig.4. SEM image of AgNPs using PELE leaf extract

3) SEM: The synthesized nanoparticle morphology was characterized by scanning electron microscope (SEM) was done by using Philips model CM 200 instrument. After the completion of reaction, the nanoparticles placed on carbon coated copper grid, it exhibit spherical in shape (Fig.4). Further, from all the SEM images it is evident that the morphology of AgNPs is nearly spherical which is in good agreement with the shape of SPR band in the UV–Vis spectra. The size of the AgNPs range around 50 -100nm [36].
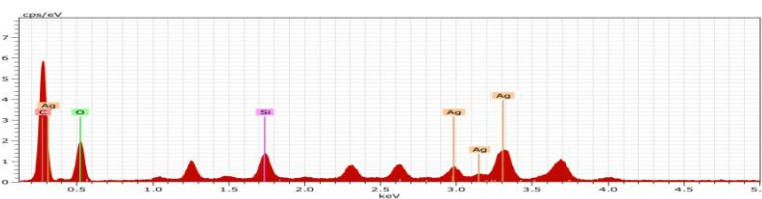

Fig.5. EDX spectra of AgNPs

4) EDAX: PELE reduced silver solutions were dried, drop coated on to glass film. The EDAX pattern thus clearly shows that the AgNPs are crystalline in nature by the reduction of silver ions by using leaf broth. It expose strong signal in the silver region and confirms the formation of AgNPs (Fig.5). Metallic silver nano crystals generally show typical optical absorption peak approximately at 3 keV due to surface plasmon resonance [37]. Other elemental signals are recorded possibly due to elements from enzymes or proteins present within the PELE.

5) XRD: The XRD pattern of the AgNPs is as shown in Fig. 6 and Table 1. The prominent diffraction peaks observed are indexed to (1 0 0), (1 0 1), (1 0 3), (0 0 6), (1 1 0) and (2 0 2) reflections of face centered cubic structure of metallic silver, respectively revealing that the synthesized AgNPs are composed of pure crystalline silver (JCPDS file no. 87-0598).
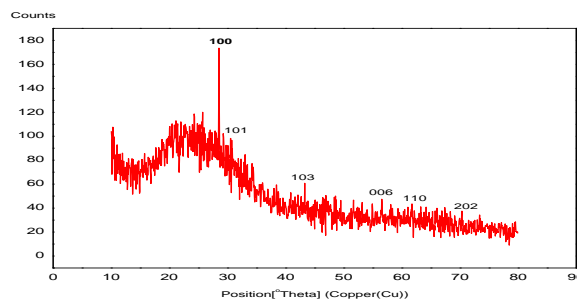

Fig. 6. X-ray diffraction pattern of AgNPs

TABLE 1

XRD PROFILE OF AgNPs

Peak Pos. [°2Th.]	FWHM Left [°2Th.]	d-spacing, [Å]	hkl values	Crystallite size [nm]
28.3873834	0.2	3.46911	1 0 0	18.53
30.8462905	0.08	3.12773	1 0 1	42.85
43.3207463	0.28	2.99868	1 0 3	13.83
56.3349622	0.16	2.77329	0 0 6	29.42
61.592655	0.09	2.65427	1 1 0	58.29
70.2087961	1.22	2.43529	2 0 2	5.54
Average crystallite size (nm)				**28.07**

The relative intensity of the (1 0 0) plane to (2 0 2) diffraction peaks in the figure was higher than the conventional value. This indicates that the prepared AgNPs may be enriched in (1 1 1) facets and thus the (1 1 1) plane seems to be preferentially oriented parallel to the surface of the supporting substrate [38]. The average particle size of AgNPs can be calculated using Debye–Scherrer equation: $D = k\lambda/\beta\cos\theta$, where D is the thickness of the nanocrystal, k is a constant, λ is

the wavelength of X–rays and β is the full width at half maxima of (111) reflection at Bragg's angle 2θ. The average particle size calculated from the XRD patterns is 28.07 nm and it is in good agreement with the particle size assigned from the SEM studies.
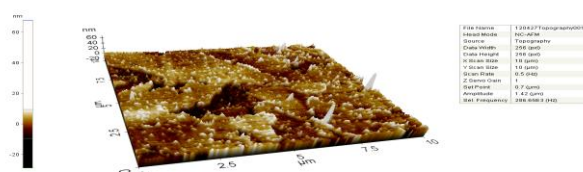

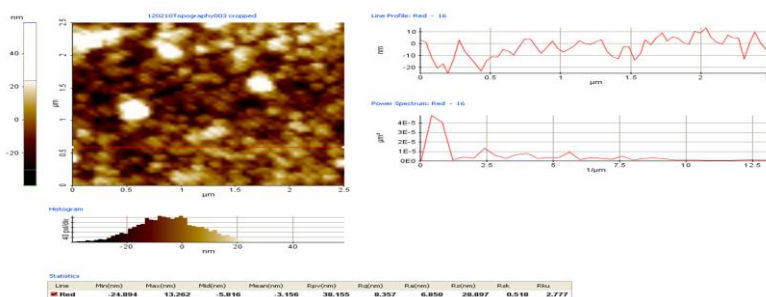Fig. 7. AFM topographical image of AgNPs
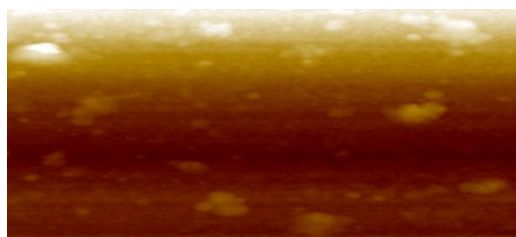

Fig. 8. AFM size distribution image of AgNPs

Fig. 9. AFM inset image of AgNPs

6) AFM: AFM analysis predominantly assures the homogeneity and the respective size of the synthesized particles. Here, the AgNPs reduced by PELE were characterized by AFM for confirming its detail size, morphology and agglomeration of the particles. From all the figures (Figs. 7, 8 and 9), it has been notified that the biologically reduced nanoparticles are in the range of 60 nm. Further, the clear particle shape of the nanoparticles is also observed from their surface topography (Fig. 8). The size distribution of the synthesized AgNPs is showed in the histogram, which ranges from 3 to 20 nm. The nanoparticles are maximum at 10nm is also showed in the line profile. The statistics graph is also showed that the size distribution of nanoparticles, this ranges from around 30 to 40 nm. In addition, the uniform spherical nature of our

synthesized nanoparticles is also confirmed from the inset image observed from AFM (Fig. 9). Thus, from the AFM observations, it is clearly confined that the synthesized nanoparticles are formed without agglomeration and are spherical in nature. All the results achieved here are in good agreement with the spectral and XRD pattern analysis [39].

7) TGA: The weight loss of AgNPs during the heating process was investigated Fig. 10. The TG curve of AgNPs revealed weight loss at two regions corresponding to the loss of water (8% by weight) at temperature around 100^oC and the loss of organic binder (50% by weight) at the temperature range of 200–500°C. Such total weight loss at 30–500°C of TG curve related to the total weight of organic binder added. No further significant weight loss peak was observed in the temperature range above 500°c. It can be concluded that AgNPs exhibited thermal stability during the heating process at the temperature range 500°C.

8) DTA: Fig. 11 shows the loss of water and organic binder of AgNPs was evidenced by One endothermic and exothermic peak around 100 and 480°C corresponding to the evaporation of water and the oxidation of organic binder. From DTA curve, it is concluded that the limiting temperature for the safer use of AgNPs was 100°C since the AgNPs degrade thermally after 100°C [40].

B .Effect of concentration and adsorption isotherm

The adsorption of Hg (II) onto the AgNPs at different Hg (II) concentrations is depicted in Fig. 12. It was observed that the adsorption of Hg (II) onto the AgNPs decreased with rise in concentration of Hg (II) from 30 to 150 mg L^{-1}. This is attributed to the greater driving force through a higher concentration gradient at high metal ion concentration [41]. Thus the developed AgNPs can be efficiently used for the removal of high concentration Hg (II) from aqueous solutions. The surface property and affinity of AgNPs for Hg (II) removal can be determined using the different adsorption isotherm models. The obtained equilibrium data from the adsorption of Hg (II) onto the AgNPs fitted to the linear equation of Langmuir [42], Freundlich [43] isotherm models. The linear equation for Langmuir and Freundlich isotherm models are expressed as follows:

$$\text{Freundlich isotherm} \quad : \log q_e = \log K_F + (1 / n) \log C_e \quad \text{------- (2)}$$
$$\text{Langmuir isotherm} \quad : (C_e / q_e) = (1 / Q_o b) + (C_e / Q_o) \quad \text{-------- (3)}$$
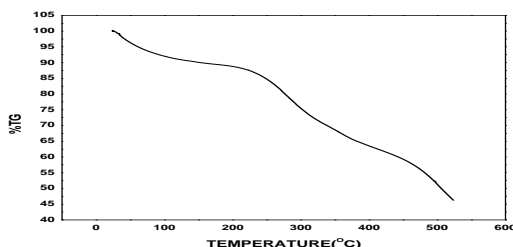

Fig. 10. TG curve of the AgNPs at different temperatures
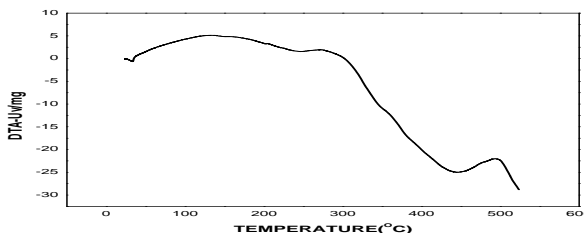
Fig. 11. DTA curve of the AgNPs at different temperatures

Where K_F (mg g^{-1}) is the Freundlich constant and 'n' the freundlich exponent. Where q_e (mg g^{-1}) is the adsorbed amount of Hg (II) at equilibrium, C_e (mg L^{-1}) is the equilibrium concentration of Hg (II), Q_0 (mg g^{-1}) and b (L mg^{-1}) are Langmuir constants related to adsorption capacity and energy of adsorption . Further, the essential characteristics of the Langmuir isotherm can be described in terms of a dimensionless constant *viz.,* separation factor or equilibrium parameter, R_L, which is defined by the equation [44].

$$R_L = 1/ (1+bQ_o) \qquad\qquad \text{------- (4)}$$

TABLE 2

NATURE OF ADSORPTION ISOTHERM AND THE FEASIBILITY OF ADSORPTION PROCESS

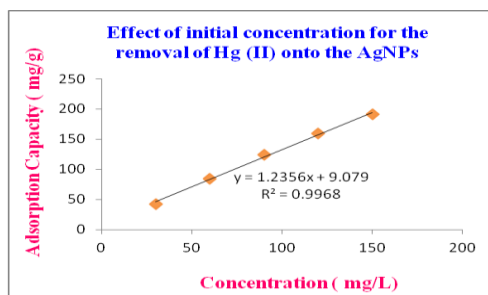| R_L value	Adsorption process
$R_L > 1$	Unfavourable
$R_L = 1$	Linear
$0 < R_L < 1$	Favourable
$R_L = 0$	Irreversible

Fig.12. Effect of concentration on the removal of Hg (II) from aqueous solution (AgNPs dose: 0.025 g, temp.: 30ºC, and Time: 30 min)
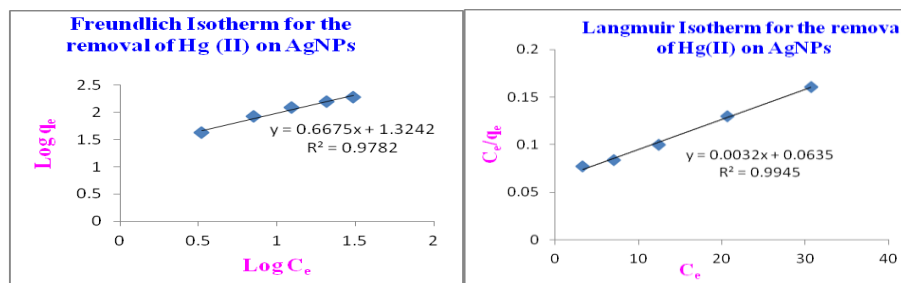

Fig.13a and b. Freundlich and Langmuir plots for the removal of Hg (II) from aqueous solution

TABLE 3
ADSORPTION ISOTHERM PARAMETERS FOR THE ADSORPTION OF Hg (II) FROM AQUEOUS SOLUTION ONTO THE AgNPs.

Metal ion	Langmuir				Freundlich		
	Q_o (mg/g)	b (g/l)	$R_L=1/1+Q_ob$	R^2	n	K_F	R^2
Hg (II)	312	0.0504	0.0597	0.9945	1.4981	21.09	0.9782

The value of R_L infers the nature of adsorption isotherm and the feasibility of adsorption process are indicated in table 2. A number of scientists have applied the Langmuir isotherm to test the formation of monolayer of adsorbate/solute, as well as the nature and the favorability of the adsorption process using R_L values.

The all values of applied adsorption isotherm parameters are calculated from their respected plots, which are included here in Fig. 13a and b, reported in Table 3. R_2 values indicated that Langmuir isotherm model for the Hg (II) adsorption was best fitted in comparison with Freundlich isotherm models. The n value was found to be 1.4981 for the Hg (II) adsorption onto the AgNPs from aqueous solution. These values are suggesting that AgNPs is better adsorbent for the separation and removal of Hg (II) from aqueous solution.

TABLE 4
COMPARISON OF ADSORPTION CAPACITIES OF DIFFERENT ADSORBENTS WITH AgNPs NANOPARTICLES

Adsorbent	Hg (II)	Reference
Expanded perlite	8.46	[46]
Thiol functionalized Fe_3O_4	227	[47]
Ethylenediamine modified peanut shells	30.78	[48]
Rice husk [47]	303.03	[49]
AgNPs	312	Present work

The values of R_L are observed to be fraction i.e., in the range of 0 to 1 (0.0504) which indicate that the adsorption process is favorable for all these adsorbents. The obtained results for the Hg adsorption are similar to the reported adsorbent by T. Sheela [45]. The adsorption capacity of the AgNPs and other adsorbents for the separation and removal of Hg (II) from aqueous solution or wastewater are tabulated in Table 4. The adsorption capacity of the AgNPs for the Hg (II) adsorption from aqueous solutions is higher than the other reported adsorbents in the literature [46–49].

C. Effect of contact time and adsorption kinetics

  The obtained data for the Hg (II) removal from aqueous solution using the AgNPs is presented in Fig. 14. The adsorption of Hg (II) from aqueous solution onto the AgNPs was rapid at the start of experiment and then rate of adsorption become slowly down. The maximum amount of Hg (II) from aqueous solutions was adsorbed onto the AgNPs within 30 min and then no significant change was observed. Thus the time of equilibrium for the Hg (II) adsorption onto the AgNPs from aqueous solutions was 30 min. The reason for rapid adsorption of Hg (II) onto the AgNPs from aqueous probable solution may be more available active sites in the AgNPs for adsorption. However the more active sites may not be available in the AgNPs for further metal ions adsorption with progress of contact time. The pseudo-first-order and pseudo-second-order kinetic models were applied to determine the adsorption rate of Hg (II) onto the AgNPs. The linear equation for pseudo-first-order kinetic model can be expressed as [50]:

$$\log (q_e - q_t) = \log q_e - [k_1 / 2.303]\ t \qquad \text{------------- (5)}$$
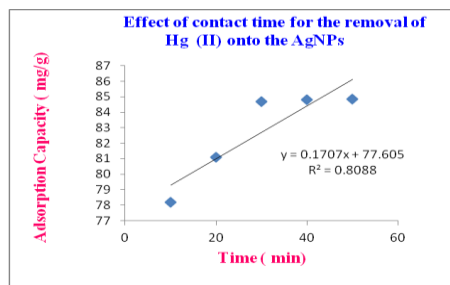
Fig. 14. Effect of contact time on the removal of Hg (II) from aqueous solution (AgNPs dose: 0.025 g, temp.: 30°C, and conc.: 60 mg L^{-1}).
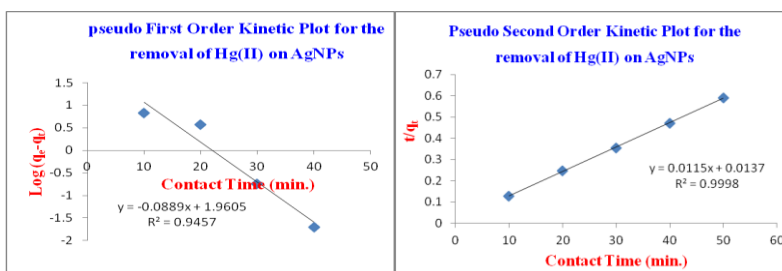

Fig.15a and b. Pseudo first and Pseudo second order plots for the removal of Hg (II) from aqueous solution

TABLE 5

THE KINETIC PARAMETERS FOR THE ADSORPTION OF Hg (II) FROM AQUEOUS SOLUTION ONTO THE AgNPs

Metal ion	Experimental q_e (mg/g)	Pseudo-I-Order constants			Pseudo-II-Order constants		
		q_e (mg/g)	K_1 (min^{-1})	R^2	q_e (mg/g)	K_2 (g/mg/min)	R^2
Hg (II)	84.85	91.3	0.2047	0.9408	86.95	9.65×10^{-3}	0.9998

Where k_1 is the pseudo-first-order rate constant (min^{-1}) and qe (mg g^{-1}) is the adsorption capacity at equilibrium and qt (mg g^{-1}) is the adsorbed amount of metal ion after time t (min). The linear equation for pseudo-second-order kinetic model can be expressed as [51]:

$$t / q_{t} = 1/ k_2 \, q_e^2 + t/q_e \hspace{3cm} \text{------------- (6)}$$

Where k_2 is the pseudo-second-order rate constant (g mg^{-1} min^{-1}). The q_e, k_1, k_2 and R_2 values for different concentrations of Hg (II) solutions were calculated from their respected plots, which are included here in Fig. 15a and b. The obtained q_e, k_1, k_2 and correlation coefficient (R_2) values are tabulated in Table 5. The R_2 values for pseudo second- order kinetic model are relatively higher than pseudo-first order kinetic model for the Hg (II) adsorption. However, the experimental qe values are very close to the calculated q_e values for pseudo-second-order kinetic model. These results implied that the adsorption of Hg (II) onto the AgNPs obeyed second order model kinetic model [52].

D. Intra-particle diffusion model (Waber–Morris model)

The overall reaction kinetics for the adsorption of Hg (II) is a pseudo-second-order process. However, this could not highlight on the rate-limiting step. The rate-limiting step (slowest step of the reaction) may be either the boundary layer (film) or the intra-particle (pore) diffusion of solute on the solid surface from bulk of the solution in a batch process. The probability of the intra particle diffusion was explored by using the following equation suggested by Weber and Morris [53].

$$q_t = k_{id} t^{1/2} + c \qquad \text{------------- (7)}$$
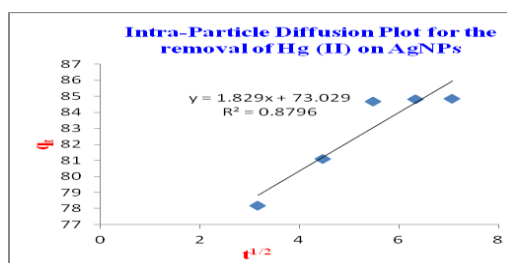

Fig. 16. Weber–Morris intra particle diffusion model for the removal of Hg (II) from aqueous solution using the AgNPs

TABLE 6

THE INTRA PARTICLE DIFFUSION PARAMETERS FOR THE ADSORPTION

OF Hg (II) FROM AQUEOUS SOLUTION ONTO THE AgNPs

Metal ion	Intra particle diffusion model		
	K_{id} (g mg^{-1} min$^{-1/2}$)	C	R^2
Hg (II)	1.829	73.02	0.8807

Where q_t is adsorption capacity at any time t and k_{id} is the intra particle diffusion rate constant (mg/g min½) and C is the film thickness. Greater the value of C greater is the effect of boundary layer on adsorption process. If the rate limiting step be the intra-particle diffusion, the plot of q_t against the square root of time should be a straight line and pass through the origin. The deviation of the plot from the linearity indicates the rate-limiting step should be boundary layer (film) diffusion controlled. It can be seen from Fig. 16 that the plots possess multi-linear portions; it indicates that the two or more steps influence the sorption process. It was found that two straight lines relate the points, the sharp first linear portion is due to the film diffusion and the second linear portion is due to the pore diffusion. Non-linearity of the plots had indicated the multi stage adsorption of Hg (II) by AgNPs nanoparticles. The extrapolation of the first linear portion gives the intercept equal to the boundary layer thickness or film thickness. The obtained $K_{id,}$ C and correlation coefficient (R^2) values are tabulated in Table 6.

E. Thermodynamics of Hg adsorption

The effect of temperature on the adsorption of Hg from aqueous solution onto the AgNPs was performed to evaluate the influence of metal ion adsorption capacity. The adsorption capacity of the AgNPs was reduced to 80.448 from 84.67 mg g^{-1} for Hg (II) with increase in temperature (30–50 ^{o}C). This may be due to the deformation of the active sites in the AgNPs with increase in temperature. Thermodynamic studies were performed in detail to find out the nature of adsorption process. Thermodynamic parameters such as standard free energy change (ΔG^o), enthalpy change (ΔH^o) and entropy change (ΔS^o) were calculated using the following equations [54]:

$$K_C = C_{ad} \text{ (solid) / } C_e \text{ (solution)} \qquad \text{------------ (8)}$$

$$\Delta G^\circ = -2.303 \, RT \log K_C \qquad \text{------------- (9)}$$

$$\text{Log } K_C = - [\Delta H^\circ / 2.303 \, RT] + (\Delta S^\circ / 2.303 R) \qquad \text{------------- (10)}$$

TABLE 7

THE THERMODYNAMIC PARAMETERS FOR ADSORPTION OF Hg (II) ON AgNPs

Temperature	$-\Delta G^o$ (kJ mol^{-1})			$-\Delta S^o$ (J mol^{-1}K^{-1})	$-\Delta H^o$ (kJ mol^{-1})
	30°C	40°C	50°C		
Hg (II)	7.23	6.88	6.74	81.31	33.33

Where K_c is the distribution coefficient, T is the temperature (K) and R is gas constant (8.314 J mol^{-1} K^{-1}). The ΔH^o and ΔS^o values were obtained from the slope and intercept of ln K_c vs. 1/T plot for the Hg (II) adsorption from aqueous solution onto the AgNPs at various temperatures. The obtained values are tabulated in Table 7. The negative ΔG^o values suggested that the adsorption of Hg (II) from aqueous solution onto the AgNPs was spontaneous in nature. The negative ΔH^o values confirmed the exothermic nature of Hg (II) adsorption. Moreover negative ΔS^o value showed reduction in affinity of Hg (II) onto the AgNPs.

IV.CONCLUSION

In this work, have built-up a simple and green method to synthesize AgNPs with diameters in the range of 50–100nm using the PELE as reductant and capping agent. The PELE has a syndicate effect of reducing the silver salt solution and also hindering the particle growth. This green chemistry approach toward the synthesis of AgNPs was trouble-free and suitable to handle, and it is understood that it has advantages over other biological syntheses. The reduction of silver ions and stabilization of the AgNPs occur through the participation of PELE compounds like tannins and flavonoids. Most importantly, the reaction was simple and convenient to handle, and it is believed that it has advantages over other biological syntheses. The present study also reports the adsorption of Hg (II) from aqueous solution onto the AgNPs was dependent on the metal ion concentration, contact time and temperature. The adsorption isotherm experiments revealed that adsorption of Hg (II) from aqueous solution onto the AgNPs was fitted well for Langmuir model. The maximum adsorption of Hg (II) from aqueous solution onto the AgNPs was found to be 312 mg/ g. The lower values of RL (0.0597) indicate that the adsorption process is favored on AgNPs nanoparticles. Kinetic studies demonstrated that the mechanism for adsorption of metal ions followed the pseudo-second-order rate model, which provided the best fit for the experimental data. Intra-particle diffusion model suggested that the initial adsorption rate controlled by the film diffusion, which followed by the pore diffusion. The thermodynamic studies revealed that the adsorption is spontaneous and exothermic for Hg (II) ions onto AgNPs. The negative entropy indicates a decrease in the degree of freedom for the adsorbed species and suggests that there is a decrease in the concentration of adsorbate in solid–solution interface.

ACKNOWLEDGEMENT

REFERENCES

[1] Philip, D., "Green synthesis of gold and silver nanoparticles using Hibiscus Rosa sinensis", Physica E, vol.42, pp.1417–1424, 2010.

[2] Rao, M.L., and Savithramma, N., "Biological Synthesis of Silver Nanoparticles using Svensonia Hyderabadensis Leaf Extract and Evaluation of their Antimicrobial Efficacy", J. Pharm. Sci. & Res, vol.3, pp.1117-1121, 2011.

[3] Geethalakshmi, R., and Sarada, D.V.L., "Synthesis of plant-mediated silver nanoparticles using Trianthema decandra extract and evaluation of their anti microbial activities", IJIRSET, vol.2, pp.970-975, 2010.

[4] Nagajyothi, P.C., and Lee, K.D., "Synthesis of Plant-Mediated Silver Nanoparticles Using Dioscorea batatas Rhizome Extract and Evaluation of their Antimicrobial Activities", J.Nano Mat, vol.10, pp.1155-2011, 2011.

[5] Prasad, T.N.V.K.V., and Elumalai, E.K., "Biofabrication of Ag nanoparticles using Moringa oleifera leaf extract and their antimicrobial activity", Asian Pac J Trop Biomed, vol.1 (6), pp.439-443, 2011.

[6] Mahitha, B., Deva, B., Raju, P., Dillip, G.R., Reddy, C.M., Mallikaruna, K., Manoj, I., Priyanka, S., Rao, K.J and Sushma, N.J., "Biosynthesis, Charecterization and antimicrobial studies of AgNPs extract from Bacopa monniera whole plant", Dig J Nanomater Biostruct, vol.6, pp.135-142, 2011.

[7] Prathna, T.C., Chandrasekaran, N., Raichur, A. M., and Mukherjee, A., "Biomimetic synthesis of silver nanoparticles by Citrus limon (lemon) aqueous extract and theoretical prediction of particle size", Colloids Surf B, vol.82, pp.152–159, 2011.

[8] Kouvaris, P., Delimitis, A., Zaspalis, V., Papadopoulos, D., Tsipas, S.A., and Michailidis, N "Green synthesis and characterization of silver nanoparticles produced using Arbutus unedo leaf extract", Materials Lett, vol.76, pp.18-20, 2012.

[9] Krishnaraj, C., Jagan, E.G., Rajasekar, S., Selvakumar, P., Kalaichelvan, P.T., and Mohan, N., "Synthesis of silver nanoparticles using Acalypha indica leaf extracts and its antibacterial activity against water borne pathogens", Colloids Surf B, vol.76, pp.50-56, 2010.

[10] Ali, D.M., Thajuddin, N., Jeganathan, K., and Gunasekaran, M., "Plant extract mediated synthesis of silver and gold nanoparticles and its antibacterial activity against clinically isolated pathogens", Colloids Surf B, vol.85, pp.360–365, 2011.

[11] Udayasoorian, C., Kumar, R.V., Jayabalakrishnan, M., "Extracellular synthesis of silver nanoparticles using leaf extract of Cassia auriculata", Dig J Nanomater Biostruct, vol.6 (1), pp.537-543, 2011.

[12] Naiya, T.K., Bhattacharya, A.K and Das, S.K "Removal of Cd (II) from aqueous solutions using clarified sludge", J. Colloid Interface Sci, vol.325, pp.48–56, 2008.

[13] Wu, X.W., Ma, H.W., Li, J.H., Zhang, J., and Li, Z.H., "The synthesis of mesoporous aluminosilicate using microcline for adsorption of mercury (II)", J. Colloid Interface Sci, vol.315, pp.555–561, 2007.

[14] Mauchauffee, S., and Meux, E., "Use of sodium decanoate for selective precipitation of metals contained in industrial wastewater", Chemosphere, vol.69, pp.763–768, 2007.

[15] Melita, L., and Popescu, M., "Removal of Cr (VI) from Industrial water effluents and surface waters using activated composite membranes", J. Membr. Sci, vol.312, pp.157–162, 2008.

[16] Basha, C.A., Bhadrinarayana, N.S., Anantharaman, N., and Meera Sheriffa Begum, K.M., "Heavy metal removal from copper smelting effluent using electrochemical cylindrical flow reactor", J. Hazard. Mater, vol.152, 71–78, 2008.

[17] Xiong, C.H., and Yao, C.P., "Study on the adsorption of cadmium (II) from aqueous solution by D152 resin", J. Hazard. Mater, vol.166, pp. 815–820, 2009.

[18] Xiong, C.H., and Yao, C.P "Adsorption behavior of gel-type weak acid resin (110-H) for Pb^{2+}", Trans. Nonferrous Met. Soc. Chin, vol.18, pp.1290–1294, 2008.

[19] Kobya, M., Demirbas, E., Senturk, E., and Ince, M., "Adsorption of heavy metal ions from aqueous solutions by activated carbon prepared from apricot stone", Bioresour Technol, vol.96, pp.1518-1521, 2005.

[20] Oubagaranadin, J.U.K., and Murthy, Z.V.P., "Adsorption of divalent lead on a montmorillonite illite type of clay", Ind Eng Chem Res, vol.48, pp.10627-10636, 2009.

[21] Sun, S., Wang, L., and Wang, A., "Adsorption properties of crosslinked carboxymethyl chitosan resin with Pb(II) as template ions", J Hazard Mater, vol.136, pp.930-937, 2006.

[22] Wang, X., Zheng, Y., and Wang, A., "Fast removal of copper ions from aqueous solution by chitosan-g-poly (acrylic acid)/attapulgite composites", J Hazard Mater, vol.168, pp.970-977, 2009.

[23] Gao, C., Zhang, W., Li, H., Lang, L., and Xu, Z., "Controllable fabrication of mesoporous MgO with various morphologies and their absorption performance for toxic pollutants in water", Cryst Growth Des, vol.8, pp.3785-3790, 2008.

[24] Lee, J., Mahendra, S., Alvarez, P.J.J., "Nanomaterials in the construction industry: A review of their applications and environmental health and safety considerations", ACS Nano, vol.4, pp.3580-3590, 2010.

[25] Xu, X., Wang, Q., and Choi, H.C., "Encapsulation of iron nanoparticles with PVP nanofibrous membranes to maintain their catalytic activity", J. Membr. Sci, vol.348, pp.231–237, 2010.

[26] Wang, Q., Qian, H.J., Yang, Y.P., Zhang, Z., Naman, C., and Xu, X.H., "Reduction of hexavalent chromium by carboxymethyl cellulose-stabilized zero-valent iron nanoparticles", J. Contam. Hydrol, vol.114 (1–4), pp.35–42, 2010.

[27] Xiong, Z., Zhao, D., and Pan, G., "Rapid and complete destruction of perchlorate in water and ion-exchange brine using stabilized zero-valent iron nanoparticles", Water Res, vol.41 (15), pp.3497–3505, 2007.

[28] Liu, T., Zhao, L., Sun, D., and Tan, X., "Entrapment of nanoscale zero-valent iron in chitosan beads for hexavalent chromium removal from wastewater", J. Hazard. Mater, vol.184 (1–3), pp.724–730, 2010.

[29] Liu, Z., and Zhang, F., "Nano-zerovalent iron contained porous carbons developed from waste biomass for the adsorption and dechlorination of PCBs", Bioresour. Technol, vol.101 (7), pp.2562–2564, 2010.

[30] Ponder, S.M., Darab, J.G., and Mallouk, T.E., "Remediation of Cr(VI) and Pb(II) aqueous solutions using supported nanoscale zero-valent iron", Environ, Sci. Technol, vol.34 (12), pp.2564–2569, 2000.

[31] Lin, C.J., Liou, S.L., and Lo, Y.H., "Degradation of aqueous carbon tetrachloride by nanoscale zerovalent copper on a cation resin", Chemosphere, vol.59, pp.1299–1307, 2005.

[32] Wu, S.J., Liou, T.H., and Mi, F.L., "Synthesis of zero-valent copper-chitosan nanocomposites and their application for treatment of hexavalent chromium", Bioresour. Technol, vol.100 (19), pp.4348–4353, 2009.

[33] Bassett, G.H., Jeffery, J., Mendham, J., and Denney, R.C., Vogel's Text Book of Quantitative Chemical Analysis, fifth ed., Longman, London,1989.

[34] Sosa, I.O., Noguez, C., and Barrera, R.G., "Optical properties of metal nanoparticles with arbitrary shapes", J. Phys. Chem, vol.107, pp.6269–6275,2003.   [35] Suman, T.Y., Radhika Rajasree, S.R., Kanchana, A and Beena, S., "Elizabeth Biosynthesis, characterization and cytotoxic effect of plant mediated silver nanoparticles using Morinda citrifolia root extract", Colloids Surf B, vol.106, pp.74– 78, 2013.   [36] Sankar, R., Karthik, A., Prabu, A., Karthik, S., Subramanian, K., and Ravikumar, V., "Origanum vulgare mediated biosynthesis of silver nanoparticles for its antibacterial and anticancer activity", Colloids Surf B, vol.108, pp.80– 84, 2013.   [37] Kannan, N., Mukunthan, K.S., and Balaji, S., "A comparative study of morphology, reactivity and stability of synthesized silver nanoparticles using Bacillus subtilis and Catharanthus roseus (L.) G. Don", Colloids Surf B, vol.86, pp.378–383, 2011.

[38] Gurusamy, A., and Cellapandian, K.., "Green Synthesis of Silver Nanoparticles using Millingtonia hortensis and Evaluation of their Antimicrobial Efficacy", Inter.j.nanomater.bios, vol.3 (1), pp.21-25, 2013.

[39] Raman, N., Sudharsan, S., Veerakumar, V., Pravin, N., and Vithiya, K., "Pithecellobium dulce mediated extra-cellular green synthesis of larvicidal silver nanoparticles", Spectrochim.*Acta* A.Mol.Biomo. Spectrosc, vol.96, pp.1031–1037, 2012.

[40] Thongnopkun, P., Jamkratoke, M., and Ekgasit, S., "Thermal behavior of nano silver clay in the application of handmade jewelry", Mater. Sci. Eng, vol.556, pp.849–854, 2012.

[41] Acemioglu, B., "Batch kinetic study of sorption of methylene blue by perlite", Chem. Eng. J, vol.106, pp.73–81, 2005.

[42] Langmuir, I., "The sorption of gases on plane surfaces of glass, mica and platinum", J. Am. Chem. Soc, vol.40, pp.1361–1403, 1918.

[43] Freundlich, H., "Uber die adsorption in loseungen", J. Phys. Chem, vol.57, pp.385– 470, 1907.

[44] Monika, J., Vinod Kumar, G., and Krishna, K., "Adsorption of hexavalent chromium from aqueous medium onto carbonaceous adsorbents prepared from waste biomass", J. Hazard. Mater, vol.91, pp.949–954, 2010.

[45] Sheela, T., Arthoba Nayaka, Y., Viswanatha, R., Basavanna, S., and Venkatesha, T.G., "Kinetics and thermodynamics studies on the adsorption of Zn(II), Cd(II) and Hg(II) from aqueous solution using zinc oxide nanoparticles", Powder.Technol, vol.217, pp.163–170, 2012.

[46] Hamid, G., Ahmad, M., Meisam, T., Parisa, Z., Mohammad Ghannadi, M., and Hossein Taheri, "Adsorption of Ag, Cu and Hg from aqueous solutions using expanded perlite", J. Hazard. Mater, vol.177, pp.950–955, 2010.

[47] Wassana, Y., Cynthia, L., and Thanapol, S., "Removal of heavy metals from aqueous systems with thiol functionalized supermagnetic nanoparticles", Environ. Sci. technol, vol.41, pp.5114–5119, 2007.

[48] Yong, L., Xiaomei, S., and Buhai, L., "Adsorption of Hg^{2+} and Cd^{2+} by ethylenediamine modified peanut shells", Carbohydr.Polym, vol.81, 335-339, 2010.

[49] Shafey, E.I., "Removal of Zn (II) and Hg (II) from aqueous solution on a carbonaceous sorbent chemically prepared from rice husk", J. Hazard.Mater, vol.175, pp.319-327, 2010.

[50] Smiciklas, I, Onjia, A., Raicevic, S., Janackovic, D., and Metric, M., "Factors influencing the removal of divalent cations by hydroxyapatite", J. Hazard. Mater, vol.152, pp.876–884, 2008.

[51] McKay, G., and Ho, Y.S., "Pseudo-second order model for sorption processes", Process Biochem, vol.34, pp.451–465, 1999.

[52] Chen, Y.H., and Li, F.A., "Kinetic study on removal of copper (II) using goethite and hematite nano-photocatalysts", J. Colloid Interface Sci, vol.347, pp.277–281, 2010.

[53] Weber, W.J., and Morris, J.C., "Equilibria and capacities for adsorption on carbon", J. of Sanitary Engineering.Division, vol.90, pp.79–107, 1964.

[54] Ahmet, S., Mustafa, T., Demirhan, C., and Mustafa Soylak, "Equilibrium, kinetics and thermodynamic studies of adsorption of Pb (II) from aqueous solution onto Turkish kaolinite clay", J.Hazard. Mater, vol.149, pp.283–291, 2007.